Proceedings of IMECE 2002:
5th International Symposium on FSI, AE, FIV & N
17-22 November 2002, New Orleans LA, USA

IMECE2002-32168

NUMERICAL SIMULATIONS OF THE FLOW-INDUCED VIBRATIONS OF TETHERED BLUFF BODIES

C.J. Pregnalato, K. Ryan, M.C. Thompson, K. Hourigan
Fluids Laboratory for Aeronautical and Industrial Research
Department of Mechanical Engineering
Monash University, Clayton VIC 3800, Australia

ABSTRACT

One of the most basic examples of fluid-structure interaction is provided by a tethered cylinder or sphere in a fluid flow. The tendency of a tethered sphere to oscillate when excited by waves is a well-known phenomenon and it has only recently been found that the same system will act in a similar fashion when exposed to a uniform flow at moderate Reynolds numbers, with a transverse peak-to-peak amplitude of approximately two diameters over a wide range of velocities. The present paper presents results of DNS of the flow past a tethered cylinder. The coupled Navier-Stokes equations and the equations of motion of the cylinder are solved using a spectral element method. The fluid forces acting on the cylinder as well as the tension in the tether are computed and used to determine the resulting motion of the object. It is found that the mean amplitude response is greatest at high reduced velocities, i.e. when the cylinder is oscillating predominantly transverse to the fluid flow. Furthermore, the oscillation frequency is found to correspond to the vortex shedding frequency of a stationary cylinder, except at high reduced velocities. This is in contrast to a tethered sphere in which the oscillation frequency does not correspond to either the vortex shedding frequency or the natural frequency. Visualizations of the vortex structures in the wake reveal the mechanisms behind the motion of the cylinder, and suggest that the induced oscillations are highly significant in the prediction of cylinder response in a steady flow.

INTRODUCTION

One of the simplest extensions to the classical problem of a hydro-elastically mounted oscillating cylinder is a cylinder whose motion is confined to an arc by a restraining tether. By considering a wide range of mass ratio, M^* (the mass of the cylinder divided by the mass of the displaced fluid), we may allow for both buoyant bodies ($M^* < 1$) and dense bodies ($M^* > 1$), and hence describe a parameter space encompassing a large and diverse range of practical applications. Despite this fact, little progress has been made regarding the fluid-structure interaction of a tethered body, and to the authors' knowledge virtually no work has been published regarding the flow around a tethered cylinder. In this work, we have developed a numerical code to simulate the interaction of a tethered cylinder in a viscous fluid. This code has been validated against preliminary experiments performed in the Monash FLAIR water tunnel.

Most previous work regarding tethered bodies has focused on the free surface interaction with tethered buoys (Harlemann and Shapiro (1961), Shi-Igai and Kono (1969), and Ogihara (1988)). In each of these studies the tethered bodies oscillate due to the combined effect of a uniform (or sheared) free stream and free surface wave effects. This combination, incorporating the interaction of a free surface, has made interpretation of results difficult.

To date, little research has been performed concerning tethered bluff bodies and only the work of Williamson and Govardhan (1997), Govardhan and Williamson (1997), and Jauvtis *et al.* (2001) deal purely with the action of a tethered body in a uniform flow. Their work dealt specifically with the motion of a tethered sphere in a uniform flow field. They found that a tethered sphere sustained large peak-to-peak oscillations with amplitudes in the order of two sphere diameters in the transverse direction. They also found smaller stream-wise oscillations of the order of about 0.4 sphere diameters.

For tethered spheres with low mass ratio ($M^* < 1$), the experimental investigation of Williamson and Govardhan (1997) found that large amplitude oscillations occurred, and

their work was extended by Jauvtis *et al.* (2001) to incorporate spheres with higher mass ratios, $M^* > 1$. In this study, four modes of shedding were observed, two of which were observed for a sphere with $M^* < 1$.

An obvious parallel to the study of tethered bodies is the investigation of the flow-induced oscillation of a hydro-elastically mounted bluff body. Significant research has been undertaken in this field, especially in regards to transversely oscillating bluff bodies. Several interesting features observed in this area lend themselves to the present investigation.

Of note is the dependence of the frequency of vortex-induced oscillation on the mass ratio (M^*) of the body. For cylinders of a high mass ratio, the vibration frequency tends to the natural frequency of the cylinder (for example, Feng (1968)). However, experiments by Angrilli *et al.* (1972) found that for cylinders with a low mass ratio ($M^* \approx 1.5$) the vibration frequency tended to the vortex shedding frequency of the flow.

In general, the mass ratio of the bluff body (M^*) and the damping ratio (λ) are often grouped as a single term (λM^*) known as the mass-damping parameter. Of interest to the present investigation are results concerning low mass-damping ($\lambda M^* \ll 1$), for example in the experiments performed by Govardhan and Williamson (2000), in which significant oscillation amplitudes (of the order of one cylinder diameter) have been noted, and three amplitude regimes exist. Note that the transition between the first two amplitude modes involves a hysteretic process.

Brika and Laneville (1993), using smoke visualization, found that as the mode of oscillation jumped from the first branch to the second, the phase difference between the cylinder displacement and the vortex shedding underwent an abrupt change. The two branches were discovered to have fundamentally different modes, namely a 2*s*- and a 2*p*-shedding mode respectively. A further mode of shedding was observed by Govardhan and Williamson (2000), when a very low mass-damped cylinder underwent flow-induced vibration.

In this paper, the numerical algorithm for simulating flow past a tethered body is presented. Solutions are obtained for a tethered cylinder and the results are discussed in the wider context of vortex-induced vibration of bluff bodies.

PROBLEM FORMULATION

The coordinate system and geometry of the problem are shown in Figure 1. For the purpose of illustration, a body of arbitrary geometry is considered without loss of generality. Note that θ is the angle formed by the plane of the tether to the x-axis, and ϕ is the angle formed by the rotation of this plane about the x-axis. For a circular cylinder, $\phi = 0$. The forces acting on the object are composed of hydrodynamic loading (drag, lift and side forces) and the tension in the tether. The buoyancy of the body (B) is combined with the pressure and viscous lift to give a net vertical force, and is denoted as $F_L + B$ in Figure 1.

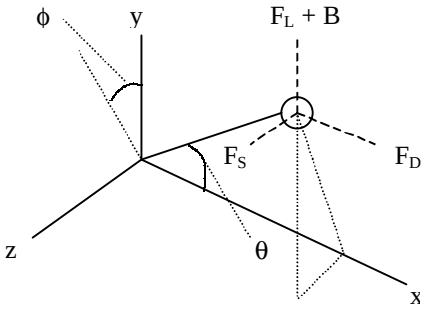

Figure 1. Schematic of a tethered body in a fluid flow.

We consider the flow of a viscous incompressible fluid past a sphere (or cylinder) under tension. The equations representing this problem are the coupled system of fluid and bluff body equations. The Navier-Stokes equations governing the fluid motion in an inertial reference frame are given by

$$\frac{\partial \boldsymbol{u}'}{\partial t} + (\boldsymbol{u}' \cdot \nabla')\boldsymbol{u}' = -\frac{1}{\rho_f}\nabla' p' + \frac{1}{Re}\nabla'^2 \boldsymbol{u}', \qquad (1a)$$

$$\nabla' \cdot \boldsymbol{u}' = 0, \qquad (1b)$$

where $\boldsymbol{u}'$ is the velocity field, p' is the pressure and $Re = Ud/\nu$ is the Reynolds number based on the sphere (or cylinder) diameter.

The tether is assumed to be rigid and inextensible (i.e., no radial movement), and the tension in it is given by

$$T = F_D \cos\theta + (F_L + B)\sin\theta\cos\phi + F_S \sin\theta \sin\phi . \qquad (2)$$

The motion of the object is a result of the forces acting on it and can be calculated from the equations

$$m\ddot{x} = F_D - T\cos\theta , \qquad (3a)$$

$$m\ddot{y} = (F_L + B) - T\sin\theta\cos\phi , \qquad (3b)$$

$$m\ddot{z} = F_S - T\sin\theta\sin\phi . \qquad (3c)$$

Combining equations (2) and (3) results in the following equations for the acceleration of the sphere in Cartesian form:

$$\ddot{x} = \frac{\gamma}{L^2 M^*}\left[\left(L^2 - x^2\right)C_D - x\left\{y\left(C_L + \left(1 - M^*\right)\alpha\right) + zC_S\right\}\right] \qquad (4a)$$

$$\ddot{y} = \frac{\gamma}{L^2 M^*}\left[\left(L^2 - y^2\right)\left(C_L + \left(1 - M^*\right)\alpha\right) - y\left\{xC_D + zC_S\right\}\right] \qquad (4b)$$

$$\ddot{z} = \frac{\gamma}{L^2 M^*}\left[\left(L^2 - z^2\right)C_S - z\left\{xC_D + y\left(C_L + \left(1 - M^*\right)\alpha\right)\right\}\right] \qquad (4c)$$

where the values of α and γ, which are geometry dependent, are listed in Table 1. Note that the parameter γ on the right

hand side of equation (4) is dimensional and has units of acceleration. For the two-dimensional counterpart (the circular cylinder), $z = C_S = 0$.

Table 1. Definition of parameters used in Equation (4).

Parameter	2-D (cylinder)	3-D (sphere)
α	$\frac{\pi}{2}\frac{gD}{U^2} = \left(\frac{\pi}{2}\frac{1}{Fr^2}\right)$	$\frac{4}{3}\frac{gD}{U^2} = \left(\frac{4}{3}\frac{1}{Fr^2}\right)$
γ	$\frac{2}{\pi}\frac{U^2}{D}$	$\frac{3}{4}\frac{U^2}{D}$

In general, the drag, lift and side forces acting on the body are computed by integrating the pressure and viscous stress terms as

$$\boldsymbol{F}(t) = \iint_S \left(-p\boldsymbol{n} + \upsilon\left(\nabla\boldsymbol{u} + \nabla\boldsymbol{u}^T\right)\cdot\boldsymbol{n}\right) ds\,, \qquad (5)$$

where the integration is performed over the surface of the object and $\boldsymbol{n}$ is the outward unit normal vector to the surface.

NUMERICAL METHOD

Solving fluid-structure interaction problems generally involves the use of deforming and/or moving meshes. For the sake of simplicity, we shall present the numerical procedure for the circular cylinder only; extension to the sphere in three dimensions is straightforward and does not necessitate additional complications.

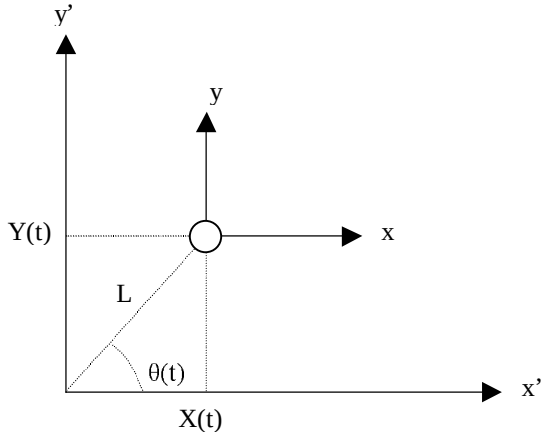

Figure 2. Transformation used to map from inertial to non-inertial reference frame.

Figure 2 shows the transformation used to map the inertial reference frame to the time-independent reference frame. This mapping is described by the following transformation

$$\boldsymbol{x} = \boldsymbol{x}' - \boldsymbol{X}(t) \qquad (6)$$

where $\boldsymbol{X}$(t) is the displacement of the cylinder and is described in terms of θ as

$$X(t) = L\cos\theta(t),\quad Y(t) = L\sin\theta(t) \qquad (7a,b)$$

In the transformed system of coordinates the cylinder appears stationary. Given the transformation (6), the Navier-Stokes and continuity equations (1a,b) become

$$\frac{\partial\boldsymbol{u}}{\partial t} + (\boldsymbol{u}\cdot\nabla)\boldsymbol{u} = -\nabla p + \frac{1}{Re}\nabla^2\boldsymbol{u} + \boldsymbol{A}(\boldsymbol{u}, p, \boldsymbol{X}) \qquad (8a)$$

$$\nabla\cdot\boldsymbol{u} = 0 \qquad (8b)$$

where the forcing term $\boldsymbol{A}(\boldsymbol{u}, p, \boldsymbol{X})$ is an additional acceleration introduced by the coordinate transformation (6) and is the acceleration of the cylinder given by (4). Due to the attachment of the coordinate system to the cylinder, the cylinder will rotate as it moves about the base pivot. Hence, the boundary conditions need to be altered in order to account for this effect.

The equations of motion for the fluid and the cylinder (or sphere) are discretized in space using a spectral element method. Typically, eighth-order Legendre polynomials were used as the tensor-product expansion basis. The equations governing the body's motion (4) are solved using a predictor-corrector technique. The Navier-Stokes and continuity equations (8) are discretized in time using a three-step time-splitting approach. The acceleration term $\boldsymbol{A}$ is combined with the non-linear terms and these are treated in the first sub step of the time update.

The coupled fluid/structure equations are solved in three steps. First, an initial angle θ is input (corresponding to an initial displacement $\mathbf{x}_0$) and the fluid equations are solved. Next, the drag, lift and side forces are computed using (5). Finally, the structure's motion is updated using (4) and the process repeated.

Detailed resolution tests were performed on a stationary cylinder to verify grid independence. A Reynolds number of Re = 500 was chosen and the order of the interpolating polynomials increased from N = 5 to N = 9. Flow quantities such as the Strouhal number, lift and drag coefficients were measured and compared to previous research. The results are summarized in Table 2. For all measures employed, the variation between the values at N = 7 and N = 9 is less than 1%. Furthermore, the values of all measures for N = 8 (used in all simulations) compare to within 1% of the numerical values of Blackburn and Henderson (1999) and Henderson (1995). Mesh independence was also verified for the moving cylinder by considering the two extremes of tether angle: at small angles, motion was predominantly in the crossflow direction, whereas at large angles, the motion was largely in the streamwise direction. For each value of N from $5 \le N \le 10$, mean tether angles, oscillation amplitudes, oscillation frequencies and drag and lift coefficients were measured for these two extreme cases. Again, all quantities compare to within 1% for the N = 8 case. A plot of the two-dimensional mesh is shown in Figure 3.

Table 2. Convergence results for a stationary cylinder. (p) denotes peak values, (m) denotes mean values.

N	5	6	7	8	9
C_L (p)	1.1873	1.1809	1.1817	1.1818	1.1854
C_L (m)	0.0383	0.0356	0.0362	0.0373	0.0434
C_D (p)	1.5897	1.5792	1.5798	1.5793	1.5795
C_D (m)	1.4561	1.4457	1.4462	1.4461	1.4459
St	0.2270	0.2264	0.2267	0.2267	0.2267

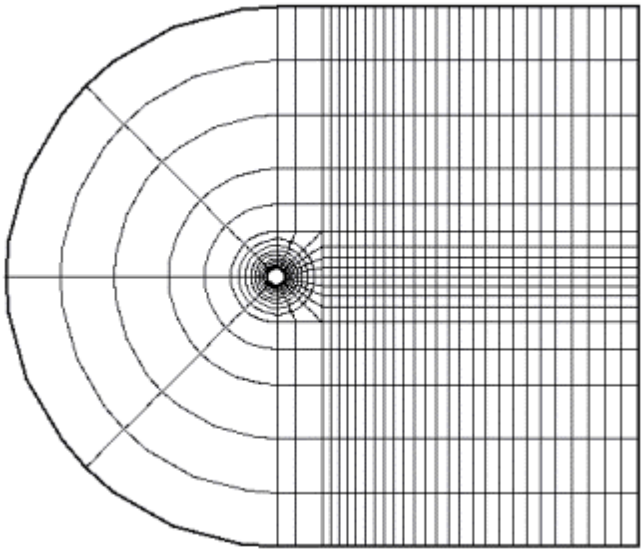

Figure 3. Two-dimensional mesh used in the numerical simulations.

RESULTS

The results presented herein involve the flow-induced vibrations of a two-dimensional circular cylinder. Predictions of the natural frequency of vibration of the cylinder can be made as follows.

Since the problem is essentially that of a pendulum with external forcing applied, the natural frequency is given by

$$f_n = \frac{1}{2\pi}\sqrt{\frac{T}{ML}}\,. \qquad (9)$$

Experimentally, the tension is assumed to be primarily dependent on the buoyancy term, in which case the normalized natural frequency may be written in terms of a Strouhal number as

$$S_n = \frac{f_n D}{U} \approx \left(\frac{1}{2\pi}\right)\frac{1}{Fr\sqrt{L^*}}\sqrt{\frac{1-M^*}{C_a+M^*}}\,, \qquad (10)$$

where C_a is the added mass coefficient for the cylinder. It is interesting to note that Equation (10) for the natural frequency of the cylinder is identical to that of a tethered sphere. However, the drag coefficient cannot be neglected for angles less than approximately 70°, in which case the equation defining S_n becomes

$$S_n = \left(\frac{1}{\sqrt{2\pi^3}}\right)\sqrt{\frac{C_D\cos\theta + \left(C_L + \left(1-M^*\right)\alpha\right)\sin\theta}{M^*L^*}}\,, \qquad (11)$$

where α is related to Fr as in Table 1.

Since the response amplitude of the cylinder is primarily a function of the reduced velocity (and is relatively independent of Reynolds number), for computational efficiency all simulations were run at a Reynolds number of Re = 200. The stronger vorticity at this Reynolds number (compared to, for instance, at Re = 100) means that a more representative determination of the vortex shedding process and hence cylinder dynamics is possible. Furthermore, both the drag coefficient and vortex shedding frequency for $200 < Re < 10^5$ is almost constant, with changes primarily in the vortex formation length.

Initially, the primary objective was to analyze the effect of mass ratio on the oscillation amplitude and frequency, since for a tethered sphere the effect of mass ratio (as well as L^* and Fr) is to influence the response shape and not necessarily the saturation amplitude. However, it was decided to study a cylinder of fixed mass ratio and tether length and see how the response (i.e., amplitude and frequency) varies with the reduced velocity. This was investigated by varying the parameter α between $1 \le \alpha \le 250$ (corresponding to normalized velocities of $4 \le U^* \le 21$) for a fixed tether length of L^* = 5.5 and a mass ratio of M^* = 0.833. These particular values were chosen to provide comparisons with preliminary experiments being conducted simultaneously in the Monash FLAIR water tunnel. Other variables of interest are the drag and lift forces acting on the cylinder, since these are the main quantities that may be compared to previous work, and the mean angle of inclination of the cylinder.

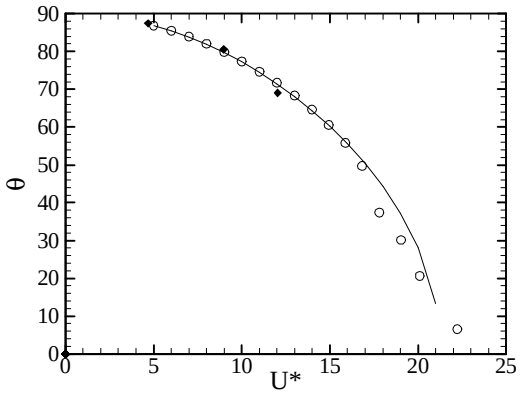

Figure 4. Mean angle of tether (in degrees): solid line denotes predicted response using equation (12); ○, numerical results; ◆, experimental results.

By considering the effect of the drag and buoyancy at equilibrium, an estimate may be made of the cylinder mean displacement. This is given by

$$\theta = \tan^{-1}\left(\frac{(1-M^*)\alpha}{C_D}\right), \qquad (12)$$

which is plotted in Figure 4 as a function of reduced velocity. Here, the value of C_D is obtained from the drag coefficient data for a stationary cylinder at the corresponding Reynolds number of Re = 200, in this case from Henderson (1995). Also shown in Figure 4 is the actual mean angle θ obtained through the numerical simulations, as well as preliminary data from the present experiments. The predicted response using (12) describes the mean angle very well, except at high reduced velocity where the mean tether angle is less than 50 degrees. This is because at these small angles, the drag for the tethered cylinder departs significantly from that of the stationary cylinder, as also shown by Blackburn and Henderson (1999) in their oscillating cylinder experiments.

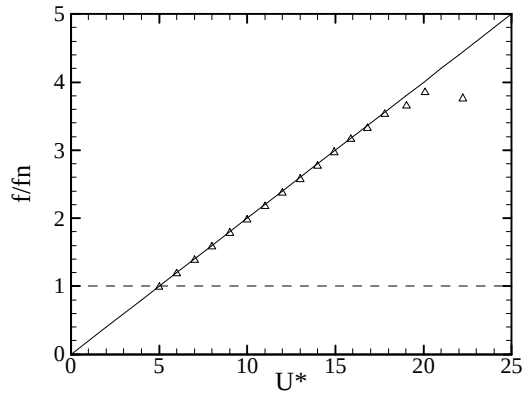

Figure 5. Normalized frequency response for M^* = 0.833, L^* = 5.5, Δ numerical results, (solid line) normalized vortex shedding frequency for a stationary cylinder (Re = 200).

Figure 5 shows the normalized oscillation for a tethered cylinder at the specified conditions (M^* = 0.833, L^* = 5.5). Also shown is the vortex shedding frequency for a stationary cylinder. As expected, it appears that the oscillations are due to a resonance between the oscillation frequency of the tethered body and the wake vortex shedding frequency. This is in contrast to a tethered sphere in which the oscillation frequency does not correspond to either the vortex shedding frequency or natural frequency at low mass ratios ($M^* < 1$). Furthermore, for a tethered cylinder the oscillation frequency for high U^* corresponds to the vortex shedding frequency and not the natural frequency of the system, similar to the response of a freely vibrating cylinder at very low mass-damping. However, no synchronization or "lock-in" regime is found when one considers the classical definition of lock-in, i.e. a synchronization of the vortex formation frequency (f_V) and body oscillation frequency (f) with the natural frequency (f), so that $f^* = f/f_N$ is close to unity, which is valid for large $M^* = O(100)$. However, a more suitable definition of synchronization would be the matching of the periodic wake vortex mode with the body oscillation frequency, as pointed out by Khalak and Williamson (1999). In this sense, the fluid force frequency must match the shedding frequency, and hence the tethered cylinder experiences synchronization throughout the entire range of reduced velocities investigated.

Cylinder oscillation amplitudes are presented in Figure 6 for the same mass ratio and tether length described above. Note that the (normalized) amplitudes are described by half of the arc length traversed by the cylinder over one period of motion. At low reduced velocities, the amplitude of oscillation is quite small, then increases almost linearly up to a reduced velocity of approximately U^* = 16.

In the range U^* = 16 to 17 there is a significant increase in amplitude. This corresponds to an increase in the drag force, above that which is observed for a stationary cylinder. In the range U^* = 17 – 19, there is a sudden drop in the displacement amplitude. While the drag force remains fairly constant throughout this range, the lay over angle is increasing and the lift force is dominating the cylinder motion. As the RMS lift force is substantially less than the RMS drag force, over the range of reduced velocities investigated, the total force tangent to the direction of motion (F_t) decreases for higher reduced velocities. Above a reduced velocity of U^* = 19, the amplitude of motion increases once again. At these very low angles of θ, the tethered cylinder responds in a similar way to a transversely oscillating hydro-elastically mounted cylinder.

To emphasize this point, a time history of the cylinder motion and the time dependent force acting tangent to the cylinder motion is presented in Figure 7 for the highest reduced velocity case simulated (U^* = 21).

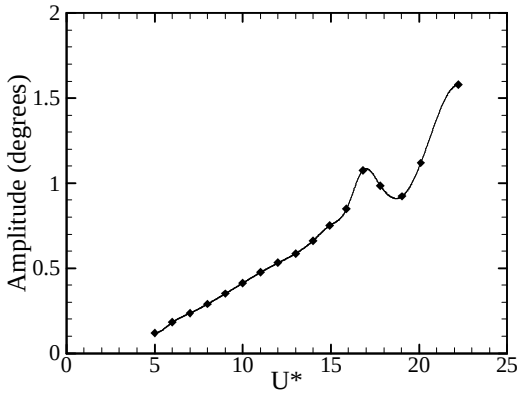

Figure 6. Cylinder oscillation amplitude as a function of reduced velocity.

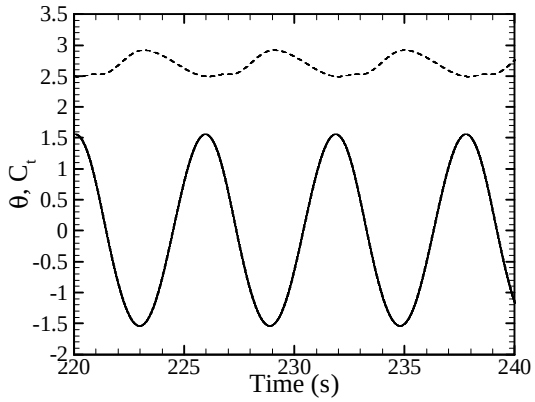

Figure 7. Tangential force coefficient (solid line) and cylinder displacement (dashed line) as a function of time for a reduced velocity of $U^* = 21$.

Figure 7 shows that the phase angle between the cylinder motion and the fluid forcing is 180°. For a very low mass-damped freely oscillating cylinder (Govardhan and Williamson (2000)), the phase angle between the displacement and forcing was 180° only on the initial branch of amplitude response. On both the upper and lower branches (as well as the lower branch for a high mass-damped oscillating cylinder which exhibits only two amplitude response branches), 2P modes of vortex formation were observed. However, the numerical prediction of 2P modes observed experimentally appears to require three-dimensional simulations, as found by Blackburn *et al.* (2001).

Figures 8 and 9 depict the vorticity field for four instances in one cycle of cylinder motion. The images in Figure 8 are for a low reduced velocity of $U^* = 5$, where the cylinder motion is predominantly in the streamwise direction, and the amplitude of motion is small. On the other hand, Figure 9 illustrates the vorticity field for a higher reduced velocity of $U^* = 21$, in which the motion of the cylinder is largely transverse to the fluid flow. In both cases, the vorticity fields clearly exhibit 2S vortex formation modes, similar to Kármán vortex shedding of a stationary cylinder at the same Reynolds number. However, the major differences between the two cases are the spacing of the shed vortices as they convect downstream and the vortex formation length in the near wake. For $U^* = 5$, the spacing between the vortices is much smaller than for $U^* = 21$. This is related to the frequency of oscillation of the body and hence the frequency of vortex shedding. In Figure 5, at low reduced velocity, the vortex shedding frequency of the tethered cylinder matches that of the stationary cylinder. However, at higher reduced velocity, there is a significant departure of the oscillation frequency from the fixed cylinder vortex shedding frequency. These lower oscillation frequencies at high U^* means that the period of vortex shedding is higher. As a result, the spacing of the vortices is much larger for high reduced velocities, as depicted in Figure 9.

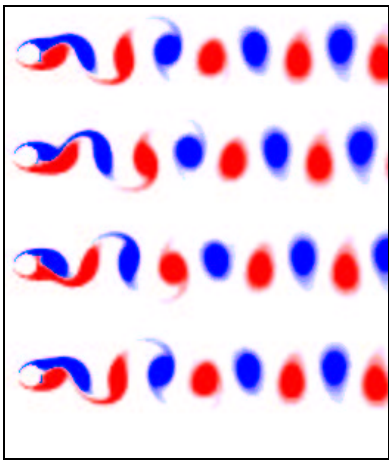

Figure 8. Vorticity field over one cycle for $U^* = 5$. Each image represents a quarter cycle.

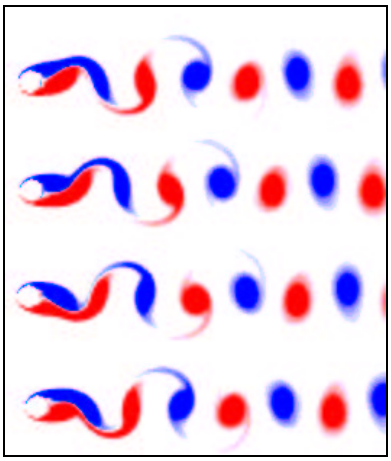

Figure 9. Vorticity field over one cycle of a fully saturated flow, $U^* = 21$. Each image represents a quarter cycle.

Future research involves examining the cylinder response for low mass ratios up to 0.9 and tether lengths in the range $5 \leq L^* \leq 20$, complemented by experimental work using similar parameters in the Monash FLAIR water channel. However, we note that a complete picture of the flow-induced vibrations of a tethered cylinder requires the implementation of three-dimensional simulations, which is a topic of future study. For example, 2P shedding modes common in vortex-induced vibrations of cylinders may be caused by three-dimensional effects, and hence two-dimensional simulations may be inadequate for the task of predicting the response and vortex shedding mechanisms (Blackburn *et al* (2001)). In addition, further work to be presented shortly considers the vortex-induced vibrations of a tethered sphere.

ACKNOWLEDGMENTS

This work is supported by the Australian Research Council. We gratefully acknowledge the support from the Victorian Partnership for Advanced Computing (VPAC) and the Australian Partnership for Advanced Computing (APAC).

REFERENCES

Angrilli, F., Di Silvo, G. & Zanardo, A. 1974 Hydro-elasticity study of a circular cylinder in a water stream. *Flow-Induced Structural Vibrations*, Naudascher (ed), Springer Berlin.

Blackburn, H.M. & Henderson, R.D. 1999 A study of two-dimensional flow past an oscillating cylinder. *J. Fluid Mech.* **385**, 255-286.

Blackburn, H.M., Govardhan, R.N. & Williamson, C.H.K. 2001 A complementary numerical and physical investigation of vortex-induced vibration. *J. Fluids Struct.* **15**, 481-488.

Brika, D. & Laneville, A. 1993 Vortex-induced vibrations of a long flexible circular cylinder. *J. Fluid Mech.* **250**, 481-508.

Feng, C.C. 1968 The measurements of vortex-induced effects in the flow past stationary and oscillating circular and D-section cylinders. Master's thesis, University of British Columbia, Vancouver BC, Canada.

Govardhan, R. & Williamson, C.H.K. 1997 Vortex-induced motions of a tethered sphere. *J. Wind Eng. Ind. Aerodyn.* **69-71**, 375-385.

Govardhan, R. & Williamson, C.H.K. 2000 Vortex modes and frequency response of a freely vibrating cylinder. *J. Fluid Mech.* **420**, 85-130.

Harlemann, D.R.F. & Shapiro, W.C. 1961 The dynamics of a submerged moor sphere in oscillatory waves. *Coast. Eng.* **2**, 746-765.

Henderson, R.D. 1995 Details of the drag curve near the onset of vortex shedding. *Phys. Fluids* **7**, 2102-2104.

Jauvtis, N., Govardhan, R. & Williamson, C.H.K. 2001 Multiple modes of vortex-induced vibration of a sphere. *J. Fluids Struct.* **15**, 555-563.

Khalak, A. & Williamson, C.H.K. 1999 Motions, forces and mode transitions in vortex-induced vibrations at low mass-damping. *J. Fluids Struct.* **13**, 813-851.

Ogihara, K. 1988 Theoretical analysis on the transverse motion of a buoy by a surface wave. *App. Ocean Res.* **2**, 51-56.

Shi-Igai, H. & Kono, T. 1969 Study on vibration of submerged spheres caused by surface waves. *Coast. Eng. Japan* **12**, 29-40.

Williamson, C.H.K. & Govardhan, R. 1997 Dynamics and forcing of a tethered sphere in a fluid flow. *J. Fluids Struct.* **11**, 293-305.